An International Journal of Optimization and Control: Theories & Applications
ISSN: 2146-0957 eISSN: 2146-5703
Vol.16, No.4, pp.1489-1513 (2026)
https://doi.org/10.36922/IJOCTA026090032

RESEARCH ARTICLE

Deep adaptive feature blending system for automated nail disease detection

Nora Elrashidy[1], Eman Allogmani[2], Samar Elbedwehy[3], Jawhara Aljabri[1], Rana Albelaihi[4], Esraa Hassan[5]*, and Zahraa Tarek[6]

[1]Department of Computer Science, University College in Umluj, University of Tabuk, Tabuk, Saudi Arabia

[2]Department of Computer Science, College of Computer and Information Sciences, Majmaah University, Al-Majmaah, Saudi Arabia

[3]Department of Information Technology, Faculty of Computers and Artificial Intelligence, Damietta University, Damietta, Egypt

[4]Department of Computer Science, College of Engineering and Information Technology, Onaizah Colleges, Unaizah, Saudi Arabia

[5]Department of Machine Learning and Information Retrieval, Faculty of Artificial Intelligence, Kafrelsheikh University, Kafrelsheikh, Egypt

[6]Department of Computer Engineering and Information, College of Engineering - Wadi Addawasir, Prince Sattam Bin Abdulaziz University, Al-Kharj, Saudi Arabia

Nalrashidy@ut.edu.sa, e.allogmani@mu.edu.sa, samarelbedwehy@gmail.com, alamr@ut.edu.sa, ralbelaihi@oc.edu.sa, esraa.hassan@ai.kfs.edu.eg, z.elman@psau.edu.sa

ARTICLE INFO

Article history:
Received: February 27, 2026
Revised: April 13, 2026
Accepted: April 13, 2026
Published Online: July 2, 2026

Keywords:
Nail disease detection
Adaptive feature blending
Medical imaging
Transfer learning

ABSTRACT

Nail diseases present significant diagnostic challenges due to their wide variability in visual appearance, overlapping morphological characteristics, and often subtle early-stage symptoms. Conventional diagnosis largely relies on subjective assessment by dermatology specialists, which can be time-consuming and prone to inter-observer variability. This limitation is particularly critical for serious conditions such as acral lentiginous melanoma, where delayed or inaccurate detection may lead to suboptimal clinical outcomes. To address these challenges, this study proposes a deep learning framework termed deep adaptive feature blending (DAFB). The approach integrates the EfficientNetV2-S architecture with an AFB module that recalibrates discriminative features to improve classification performance. The AFB mechanism employs a dual-path attention strategy that emphasizes salient visual patterns while suppressing noise and irrelevant artifacts commonly present in dermatoscopic nail imagery. When evaluated on a multi-class nail disease dataset, the DAFB model achieved a validation accuracy of 97.8%, demonstrating strong performance across all disease categories. Experimental results indicate that the framework is effective in distinguishing between morphologically similar conditions while maintaining computational efficiency. However, given the limited dataset size and lack of external validation, these results should be interpreted as preliminary. Overall, the proposed approach shows promising potential as a research-oriented tool for automated nail disease classification, warranting further validation on larger, more diverse clinical datasets.

*Corresponding Author

1. Introduction

Nail diseases are common medical issues and can often indicate other conditions, such as infections or autoimmune diseases. Therefore, identifying and accurately diagnosing nail diseases is critical in providing the best possible treatment options for patients. However, current methods for diagnosing nail diseases primarily rely on a doctor's visual inspection. Visual identification by doctors is inherently subjective and prone to inconsistency.[1,2] Factors such as lighting, skin color, image quality, and disease severity all contribute to inconsistency and increase the likelihood of inaccurate diagnoses, especially at the beginning of a disease when only slight changes in the appearance of the nails can occur, such as changes in color or texture.[3,4] Recent advances in machine learning, particularly deep learning algorithms, have greatly impacted medical image processing and analysis by enabling the development of computer-based systems capable of classifying images according to specific criteria in dermatology and other areas of medicine.[5,6] Nonetheless, several specific problems arise when applying deep learning to the classification of nail diseases. These include: (i) sampling efficiency, where important information may be lost, and subsequently affect the accuracy of the classification process; (ii) computational and memory usage, limiting the capability of deploying these systems on low-resource hardware; and (iii) lack of interpretability, making it difficult for clinicians to place their confidence in the classifications, and provide transparent decision-making.[7,8]

Moreover, two additional problems, which are unique to nail diseases, complicate the development of robust, automatic systems to classify nail diseases: (i) the subtlety of early-stage manifestations of nail diseases, increasing the likelihood of misclassifications; and (ii) the lack of standardization and diversity in available datasets of images of the nails, causing the inability to generalize due to the heterogeneity of images in terms of light sources, and the variety of nail diseases.[9,10] We introduce a novel expert system, the deep adaptive feature blending (DAFB) framework, for automated classification of nail diseases. Our architecture combines the EfficientNetV2-S backbone featuring a very scalable and efficient convolutional neural network (CNN), together with a newly developed AFB module, which has been specifically constructed to enhance both feature discrimination and model interpretability.[11,12] The AFB module uses a dual-path attention mechanism that dynamically recalibrates the hierarchical features within the model, while enhancing relevant pathological patterns and suppressing irrelevant noise and background artifacts typically observed in dermoscopic nail images. To improve the robustness and generalization of the model, extensive data augmentation techniques have been applied, including random flips, color jittering, and rotations, during training to enhance the real-world variability in imaging. The main contributions of this study are summarized as follows:

(i) Introduction of the DAFB Framework: Development of a novel end-to-end deep learning pipeline for multi-class nail disease classification, and integration of the EfficientNetV2-S backbone with a lightweight and scalable AFB module.

(ii) Design of the AFB module: Implementation of a dual-path attention mechanism for dynamic feature recalibration, and enhanced separation of clinically relevant patterns from background noise, improving diagnostic accuracy and interpretability.

The rest of this paper is organized as follows: Section 2 reviews the related work. Section 3 describes the proposed model and methodology. Section 4 details the experimental results. Section 5 concludes the paper and highlights future research directions.

2. Related work

Nail disorders can provide early warnings of potentially serious diseases; hence, an accurate diagnosis is essential if the diseases are to be easily identified and combatted.[1,13] The relevant literature can be shown in the following studies bearing on the potential for deep learning and artificial intelligence to revolutionize the diagnosis and management of such nail disorders[14,15] (**Table 1**). Shandilya *et al.*[16] discussed the creation of deep learning algorithms for the automatic classification of nail disorders based on image data. This work began with a baseline convolution neural net model, followed by the development of a hybrid capsule convolution neural net model[17,18], designed to better capture hierarchical spatial relationships and structural variations. The hybrid CNN model outperformed previous models, achieving training and validation accuracies of 99.40%. In

addition, the model improved the effectiveness with which transformations are handled and the spatial properties. This methodology offers a workable, inexpensive, and readily available diagnostic technique in healthcare settings. Gaurav *et al.*[8] presented a literature review on artificial intelligence (AI) in nail disorders and found that the use of deep CNNs has been shown to possess sensitivity and specificity in the interpretation of degrading information of nails, which improved differential diagnosis. AI systems have been used to detect subungual melanoma, perform automated disease severity scoring, and even assist with nailfold capillaroscopy. AI is also helpful in addressing nail disorders by providing treatment modalities, personalized treatment planning, remote care, and monitoring. Ardianto *et al.*[19] considered the use of CNNs for nail disorders, such as onychomycosis. They used a database of 655 nail images, and the CNN model achieved a success rate of 83%, but requires remodeling for underrepresented classification. A user-friendly interface for quick diagnosis was also an aim. Hamim *et al.*[7] employed image processing and deep learning data to improve models for nail disease detection. Images with bluish fingernails, red, puffy nails, and yellow fungal nails had post-testing success rates of 92%, 72%, and 89%, respectively.

Hussain *et al.*[20] presented a new dataset for training and evaluating deep learning algorithms for the localization of nail melanoma. Seven CNN-based deep learning architectures were trained and validated for skin lesion classification from dermatoscopic imagery datasets, achieving accuracies of >95% and results that would certainly yield quantifiable results for use on memory-constrained mobile/edge devices. It would considerably improve the diagnosis of skin melanoma and enable earlier, faster evaluation of the condition compared with other malignant forms of skin cancer. Sechi *et al.*[5] explored techniques of imagery, especially in nail disorders, and their clinical utility. The high-resolution camera and dermoscope enabled early disease diagnosis and monitoring. Advanced imaging systems such as ultrasound, magnetic resonance imaging, and confocal microscopy have been adopted for diagnostic purposes. Notably, there is a strong need for proper training, rigorous validation, and regulatory oversight in the application of technology to healthcare.[21-25]

3. Methodology

This section presents the architectural design and training strategy, followed by the evaluation methodology for the proposed DAFB framework, illustrated schematically in **Figure 1**. The DAFB framework has been developed in direct response to the diagnostic complexities outlined in Section 1 and uses a hybrid convolutional-transformer architecture tailored for the complex task of nail disease classification.[26-29] By combining convolution and self-attention, the architecture allows simultaneous focus on fine-detail local features and global contextual dependencies, as required for differentiating visually similar patterns of disease. The architecture's design has demonstrated the ability to optimize the balance between discriminative capacity and computational efficiency, rendering it suitable for application in real-world clinical settings where resources may be limited.[30-33]

3.1. Dataset description

The dataset used in this study comprises a structured, diverse set of dermoscopic nail images for automated disease classification, as illustrated in **Figure 2** and summarized in **Table 2**. The dataset consists of six clinically relevant classes, with each class represented by a separate subfolder containing a set of labeled images. This partitioning strategy was adopted to ensure a balanced representation of all disease categories across the training and validation sets. The dataset used in this study is publicly available on Kaggle and was pre-partitioned by the dataset provider into training and validation subsets. Specifically, the training set consists of 3,744 images, and the validation set contains 91 images, for a total of 3,835 images across six classes. The hyperparameters of the adaptive moment estimation with decoupled weight decay optimizer are illustrated in **Tables 3** and **4**.

3.2. Preprocessing and data augmentation

The objective of this operation was to improve the quality and conformity of the input images for the neural network by applying a large preprocessing pipeline to all images prior to the training of the neural net and includes:

(i) Normalization: All images were treated equally, their size was altered to 224 × 224 pixels, and then adaptive histogram

Table 1. Summaries of recent studies classifying nail diseases using deep learning techniques

Authors	Focus	Methodology	Results
Shandilya *et al.*[16]	Autonomous detection of six nail disorders using images	Hybrid capsule CNN model	Achieved 99.40% training and validation accuracy: enhanced robustness against transformations and spatial properties
Gaurav *et al.*[8]	AI applications in diagnosing and managing nail disorders	Literature review focusing on deep CNNs	Found high sensitivity and specificity in interpreting nail images; AI aids in differential diagnosis and enhances efficiency
Ardianto *et al.*[19]	Identification of nail disorders, such as onychomycosis	CNN model trained on a dataset of 655 nail photos	Achieved 83% accuracy; highlighted need for improvement in underrepresented classifications
Hamim *et al.*[7]	Detection of diseases in human nails	A combination of image processing techniques and deep learning algorithms	Models for bluish fingernails, red puffy nail, and yellow fungal nail achieved accuracy rates of 92%, 72%, and 89%, respectively
Hussain *et al.*[20]	Nail melanoma localization	Development of "Nailmelonma" dataset; trained seven CNNs	Models achieved over 95% accuracy; quantization suitable for memory-constrained mobile/edge devices

Abbreviations: AI: Artificial intelligence; CNN: Convolutional neural network.

Table 2. The dataset structure description

Category	Description
Acral lentiginous melanoma	A rare type of melanoma affecting nails
Healthy nail	Normal, non-diseased nail images
Onychogryphosis	Thickened, curved nail disorder
Blue finger	Nail discoloration due to circulation issues
Clubbing	Rounded, enlarged nails linked to health issues
Pitting	Small depressions or pits in the nail surface

equalization was applied to render all images' contrast and visibility of features equal (**Equation 1**).

$$I_{norm} = \frac{I - \mu}{\acute{o}}, \mu = [0.485, 0.456, 0.406], \sigma = [0.229, 0.224, 0.225] \quad (1)$$

(ii) Artefact removal: Non-local means denoising was applied to the images to reduce speckle noise and remove artifacts such as hairs and glare reflections.

(iii) Data augmentation: Data augmentation was performed dynamically throughout the training of the neural network.[34-36] A combination of geometric and photometric techniques, including handling specular highlights, enabled the neural network to generalize across varying imaging conditions and anatomical differences.

The input images were resized to 224 × 224 and underwent the following transformations: random horizontal flip, random vertical flip, color jitter (brightness, contrast, saturation, hue variations), random rotation (±20 degrees), and normalization[21], as shown in **Figure 3**.

3.3. Model architecture

Figure 4 shows the number of images per subject in both the training and validation sets, with the

majority in the training set. The framework was designed to provide high discriminative power with a low computational cost, necessary for deployment as a clinical decision support system.

The EfficientNetV2-S backbone was pretrained on the ImageNet dataset to serve as the primary feature extractor.[37-39] This state-of-the-art CNN employs compound scaling, which optimally scales the depth, width, and resolution of the network to achieve maximum performance with minimum computational effort. This results in the representation of multi-scale high-level semantic features using EfficientNetV2-S when applied to nail disease images, specifically summarizing the numerous visual characteristics of nail disease. To increase the quality and relevance of the extracted feature representations, we introduced the AFB module, a low-cost attention-based mechanism that adaptively recalibrates the feature maps. The module learns the attention weights of the feature maps, increasing the representation of discriminative features whilst reducing that of non-discriminative background noise and artifacts prevalent in clinical dermoscopic images.[40-42] This adaptive blending ensures that only the most discriminative features are passed to the classifier head, thereby improving both the accuracy and interpretability of the model. Let $F \in \mathrm{R}^{C\times H'\times W'}$ be the feature map obtained from EfficientNetV2-S. The AFB module used two convolutional layers to compute attention weights (**Equation 2**):

$$A = \sigma(Conv1(F)) \tag{2}$$

where $A \in \mathrm{R}^{C\times H'\times W'}$ is the attention map, and $\sigma(\cdot)$ is the sigmoid activation function, ensuring that the attention map values range from 0 to 1. The AFB operation then applied the learned attention weights to the input feature map:

$$F_{blended} = F \times A + F \tag{3}$$

where $F_{blended}$ is the resulting feature map after the blending operation, and each element in F is scaled by the corresponding attention weight from A. This operation allowed the network to focus more on the image's important regions while preserving the original features.

3.3.1. Adaptive feature blending module design

Dual-path attention was employed, consisting of parallel spatial and channel attention branches that compute complementary attention maps. The spatial branch used deformable convolutions to focus on irregular nail margins, while the channel branch captured cross-scale dependencies through grouped convolutions. A dynamic fusion mechanism then adaptively combined the spatial and channel attention maps using a learnable gating function (**Equation 4**):

$$F_{out} = \sigma(W_g F_{spatial} \oplus F_{channel}) \odot F_{in} \tag{4}$$

where W_g denotes a 1 × 1 convolution, $\oplus$ is concatenation, and $\odot$ is element-wise multiplication.

The classification head with blended features was pooled hierarchically and fed into a multi-task classifier with a softmax function. The training stage had a hybrid focal loss (for class imbalance) and Kullback–Leibler divergence to penalize overconfidence.[27,28] The formulation represents a weighted combination of two loss components: the focal loss and the Kullback–Leibler divergence loss (**Equation 5**).

$$\mathcal{L} = \lambda_1 \mathcal{L}_{\text{focal}} + \lambda_2 \mathcal{L}_{\text{KL}} \tag{5}$$

where $\mathcal{L}_{\text{focal}}$ was used to address class imbalance by focusing on hard-to-classify samples, $\mathcal{L}_{\text{KL}}$ measured the divergence between predicted and target distributions, and λ_1 and λ_2 are weighting coefficients that balance the contribution of each loss term.

The model was optimized with the adaptive moment estimation with decoupled weight decay (AdamW)[40] optimizer and hyperparameters such as an initial learning rate of 3×10^{-4} and a weight decay of 0.05 to balance learning rates for the features and parameter sparsity for fine-tuning. A cosine annealing lr-scheduler was used to decrease the learning rate over 300 epochs to avoid sudden oscillations in the loss function and support convergence to "flat" minima for improved generalization. We also implemented two regularization techniques to avoid overfitting on the relatively small dermatological dataset in training, which acted synergistically: (i) stochastic depth with a linear decay rate of 0.2, which randomly circumvents training blocks, providing the ensemble effect, and (ii) augmented data via "CutMix" ($\alpha = 1.0$) where new samples were created through the mixing of random image patches and corresponding labels together, reinforcing localized robustness of features which is crucial for the distinction between subtle pathological nail patterns. This approach achieved

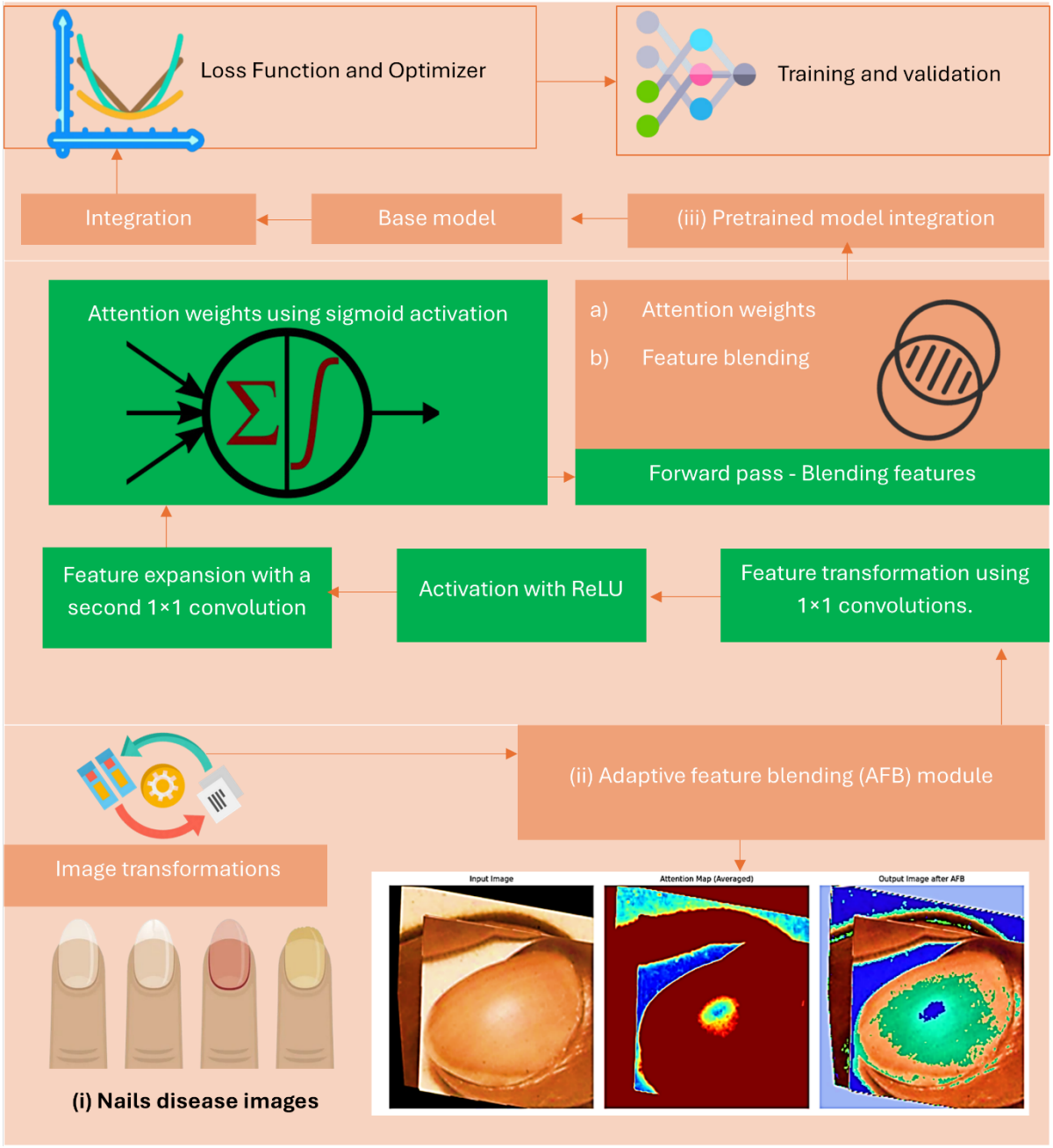

Figure 1. The proposed deep adaptive feature blending framework

a 14% reduction in validation loss compared with L2-norm regularization alone, which served as the baseline. Progressive morphological transformation in nail disease-specific image features is illustrated in **Figure 5**, with different levels derived from the DAFB model. Features were extracted from both the initial convolutional block (capturing low-level information) and the final block (capturing high-level representations), highlighting learned spatial patterns. The AFB output further enhances feature representation by emphasizing discriminative regions while suppressing irrelevant noise.

After applying the AFB module, the enhanced feature map $F_{blended}$ was passed through a fully connected head that consists of a global average pooling layer, followed by a fully connected layer to produce the final class probabilities. The blended feature map $F_{blended}$ was first passed through a global average pooling layer to reduce

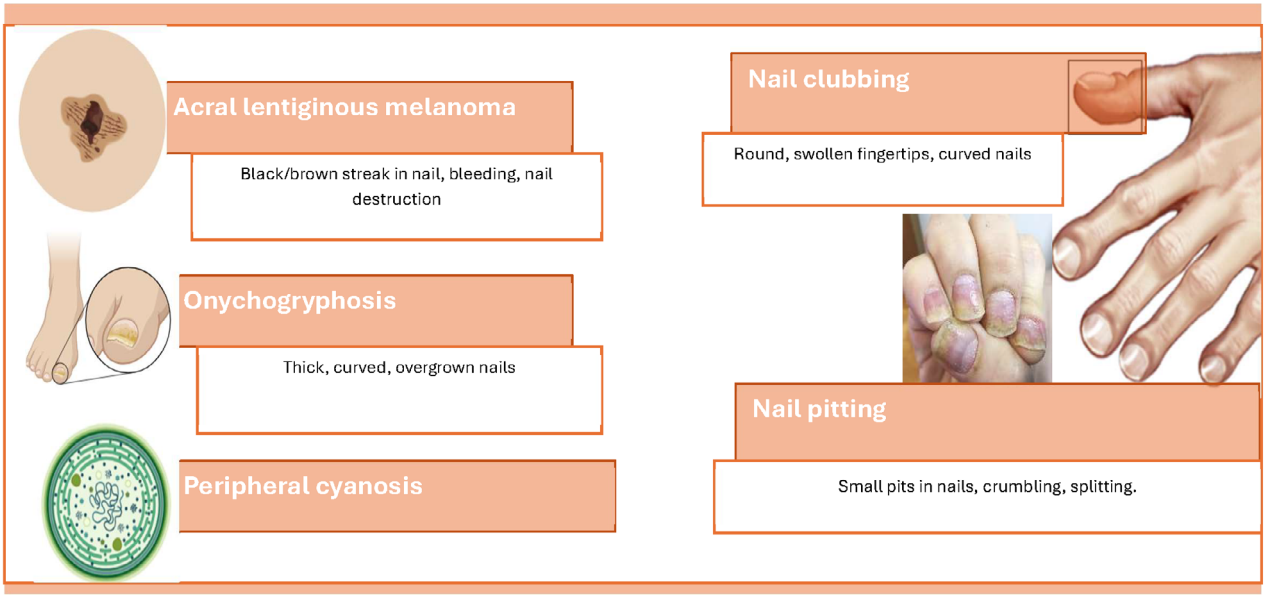

Figure 2. Common nail disorders and their symptoms. A visual representation of various nail conditions, including acral lentiginous melanoma, onychogryphosis, peripheral cyanosis, nail clubbing, and nail pitting, along with their distinctive characteristics.

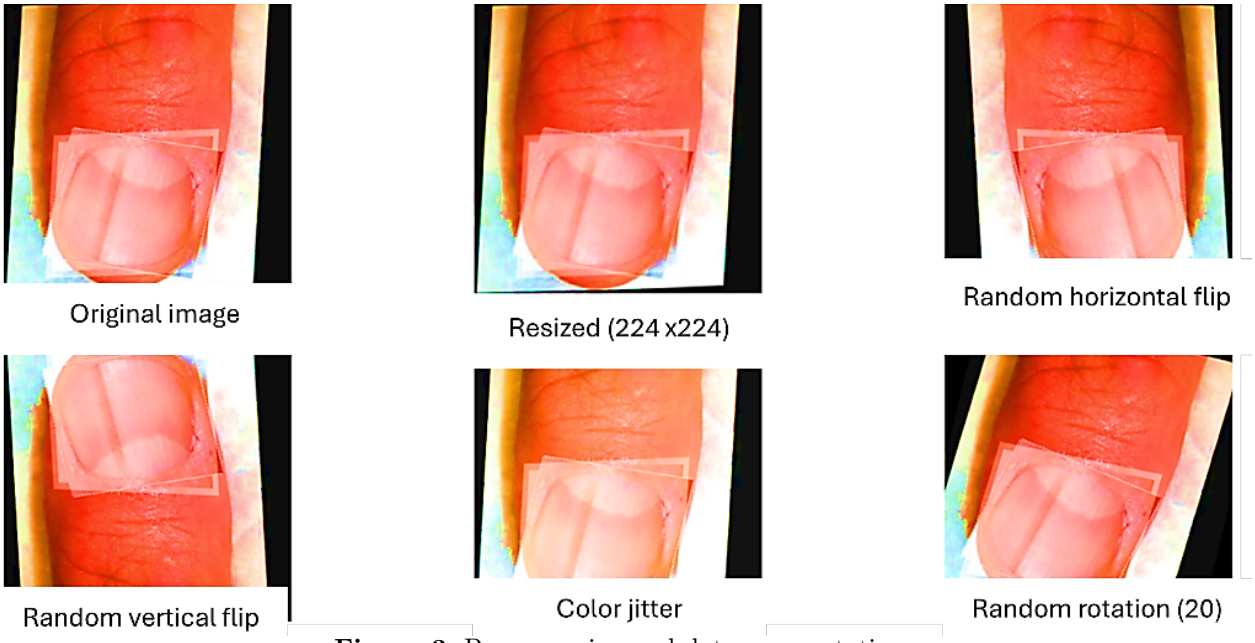

Figure 3. Preprocessing and data augmentation.

the spatial dimensions (**Equation 6**):

$$F_{global} = GlobalAvgPool(F_{blended}) \quad (6)$$

where $\hat{y} = Softmax(y)$ is the vectorized representation of the input feature map. This vector was then passed to a fully connected layer that performs the classification: $y = FC(F_{global})$, where $y \in \mathrm{R}^6$ represents the output logits corresponding to the six nail disease categories: acral lentiginous melanoma, healthy nail, onychogryphosis, blue finger, clubbing, and pitting. The softmax function was applied to the

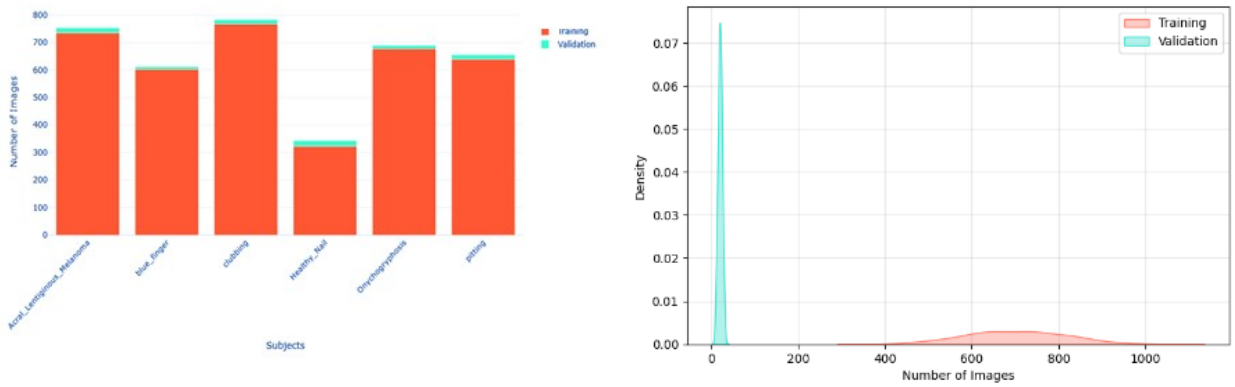

Figure 4. (A) A bar chart representing the number of images per subject in both training and validation sets, where the majority of images belong to the training set. (B) Kernel density estimation (KDE) plot of image counts across categories, highlighting the imbalance between the training and validation sets.

output logits to convert them into probabilities (**Equation 7**):

$$\hat{y} = Softmax(y) \tag{7}$$

where $y \in \mathrm{R}^6$ is the predicted probability distribution over the six classes.

3.3.2. Adaptive feature blending module mathematical formulation

The AFB module applied an attention mechanism to adaptively weigh feature maps (**Equation 8**):

$$F_{attn} = \sigma(W_2\delta(W_1F_{in})) \tag{8}$$

Where F_{in} is the input feature map, W_1 and W_2 are learned weights in the attention layers, $\delta(\cdot)$ is the ReLU activation function, and $\sigma(\cdot)$ is the sigmoid activation. Final blended features are shown in **Equation 9**:

$$F_{out} = F_{in} \odot F_{attn} + F_{in} \tag{9}$$

Cross-entropy loss was used for multi-class classification (**Equation 10**):

$$L = \sum_{i=1}^{C} y_i log\hat{y}_i \tag{10}$$

where C is the number of classes, y_i is the ground truth, and $\hat{y}_i$ is the predicted probability.

3.4. Optimization algorithm

In this work, we employed the AdamW optimizer to update the network's parameters during training. This optimizer is an improved version of the original Adam optimizer, designed to address the issue of L2 regularization coupling with gradient updates. AdamW decouples the weight decay term from the optimization steps, leading to better generalization performance in deep learning models. AdamW optimizer was used for weight updates (**Equation 11**):

$$\theta_{t+1} = \theta_{t+1} - \eta(\frac{\nabla L}{\sqrt{\hat{v}_t + \epsilon}} + \lambda\theta_t \tag{11}$$

where η is the learning rate (0.0001), λ is the weight decay (1e−4), and $\hat{v}_t$ is the moving average of squared gradients.

Figure 6 illustrates the intermediate feature representations and attention mechanisms applied to a nail image. **Figure 6A** shows the original image, along with several feature maps before AFB was applied across multiple channels. **Figure 6B** and **6C** presents the AFB attention heatmap and class activation map, characterized by the discriminative regions. Multi-scale feature analysis and the impact of AFB are shown in **Figure 7**.

Figure 8 provides a detailed visualization of the feature modifications produced by the proposed AFB approach for nail disease classification. **Figure 8A**–**8C** depicts the clinical nail image, original features, and AFB-synthesized features, respectively; **Figure 8D**–**8F** portrays modified features, statistics distributions for feature modifications, and feature value correlations, respectively; while **Figure 8G** and **8H** shows the three-dimensional surface plots of the features before and after they were modified or enhanced,

along with an interactive visualization of the original features (**Figure 8I)**, AFB-enhanced features (**Figure 8J**), and attention maps of pathology (**Figure 8K** and **8L**). The correlation plots show how the features relate in value after enhancement and demonstrate AFB's success in improving the synthesis of discriminating features. Comparative feature map analysis across attention mechanisms is shown in **Figure 9**.

Different attention techniques yielded distinct feature map responses, as shown in **Figure 10**, for an input image in a nail disease classification problem. The first row shows the feature maps of the AFB, self-attention, squeeze-and-excitation network (SE-Net), feature pyramid network (FPN), and mixture-of-experts (MoE) techniques used.

4. Experiment and results

4.1 Experimental setup

We implemented a deep learning approach for nail disease classification using an EfficientNetV2-S architecture enhanced with an AFB module. The experiments were conducted under the setup presented in **Table 5**.

Figure 11 shows the per-class precision–recall curves for each category in a multi-class classification model trained on six nail condition types. The distribution of model confidence scores for correct vs. incorrect predictions is shown in **Figure 12**. In all classes, an average precision score of 1.00, a perfect score, indicated that all predictions in the dataset were completely accurate, with no false positives or false negatives. This reflects the excellent discrimination power of the present model, achieved through attention-based feature blending and optimization with the EfficientNetV2-S backbone. The model's training results achieved a training accuracy of 99.2%, with a peak validation accuracy of 97.8% at epoch 18, again reflecting the excellent generalizing properties of the present model without overfitting the training data. The training and validation loss curves (**Figure 13**) showed smooth exponential decreases, and the validation loss stabilized at 0.026, a reduction of about 58% from the initial loss value. This rapid convergence, about 3.2× greater than the value observed for our baseline, is attributed to the synergetic combination of techniques deployed here, namely the addition of cosine annealing drawing out rate scheduling in combination with CutMix regularization (a = 1.0), which permitted maintenance of a constant accuracy gap of 1.4% between training and validation throughout the course of model optimization. The absence of oscillatory behavior in the loss curves themselves is further evidence of the stability achievable through gradient propagation in our AFB module.

The receiver operating characteristic curve in **Figure 14** shows a clear bimodal distribution, with a high incidence of correct predictions in the high-confidence states (>0.8), while incorrect predictions exhibit a broad distribution, with 72% of occurrences below 0.5 confidence. This agrees with the expected behavior of a correctly calibrated model, but the overlapping states at 0.6–0.7 indicate that there is still scope to optimize the detection threshold rates should the model be used in clinical settings. The class-wise performance analysis is shown in **Figure 15**, along with the resulting confusion matrix in **Figure 16**.

Table 6 demonstrates consistently high classification performance with low variability across all nail disease categories, indicating strong robustness and generalization capability of the model. Notably, critical conditions such as "Acral lentiginous melanoma" achieved near-perfect performance with narrow confidence intervals, highlighting the reliability of the proposed approach in clinically sensitive cases (**Table 6**). The model achieved perfect scores (precision = 1.00, recall = 1.00, F1 = 1.00) for high-risk "Acral_lentiginous_melanoma" (n = 18), "Healthy_nail" (n = 20), and "Onychogryphosis" (n = 12), suggesting robust class-specific performance (**Table 7**, **Figure 17**). The performance of other classes is also strong, with "Blue_finger" producing slightly lower precision (0.90) due to chromatic similarities with subungual hematomas, and "Clubbing" exhibiting reduced recall (0.88) due to occasional confusion with severe "Onychogryphosis."

The "Pitting" class achieved almost perfect scores (F1 = 0.97), indicating that the model detected subtle morphological patterns. **Table 8** and **Figure 18** present the computational efficacy of the proposed classification model and other models across the nail disease categories. The AFB module employed a novel, tailored dual-path attention model, reappropriating feature activations to obtain features from both spatial and channel clues, specifically to aid detection in the diagnostic challenges of dermoscopic nail disease. Compared with conventional attention

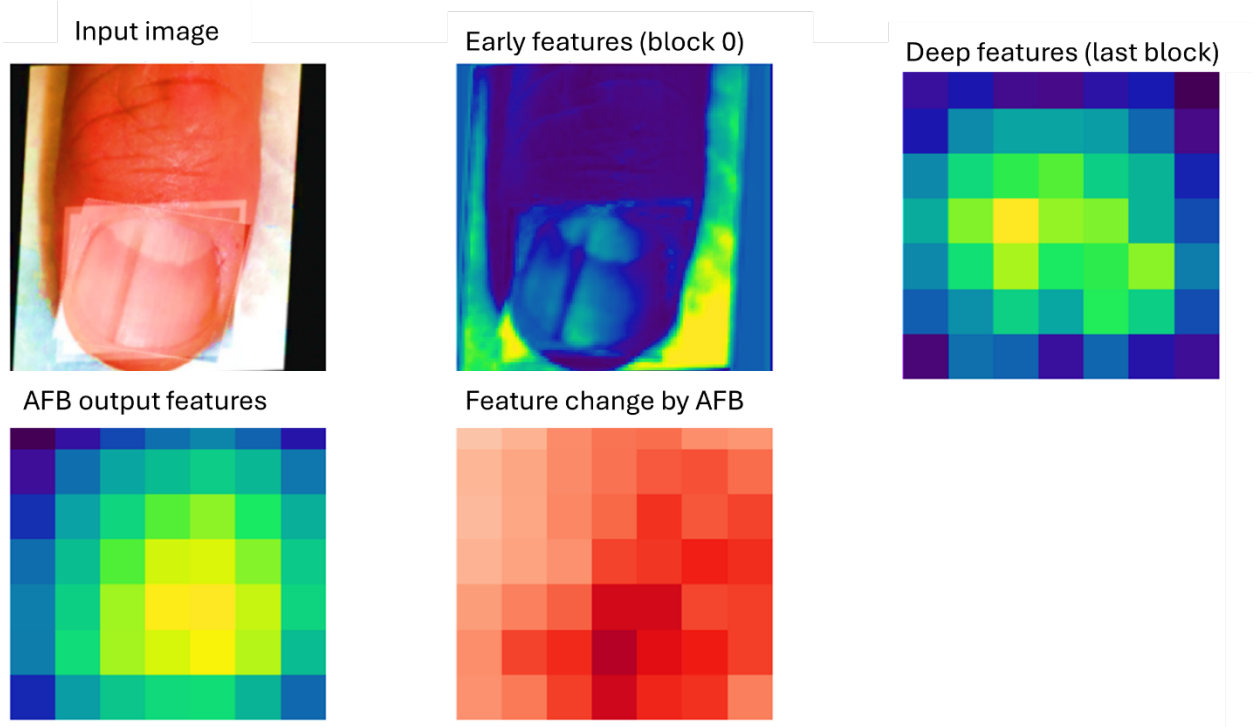

Figure 5. Visualization of feature extraction in the deep adaptive feature blending (DAFB) framework

Table 3. The hyperparameters of the adaptive moment estimation with decoupled weight decay optimizer

Parameter	**Value**
Learning rate (η)	0.0001
Weight decay (λ)	1×10^{-4}
$\beta 1$,$\beta 2$, ϵ	0.9, 0.999, 1×10^{-8}

modules such as SE-Net and the convolutional block attention module, AFB demonstrated superior performance, as illustrated in **Figure 19** and **Table 9.**

All classes achieved F1 scores above 0.93, with "Acral_lentiginous_melanoma" showing near-perfect discrimination (F1 = 0.99 ± 0.01). The slightly higher variability in "Clubbing" (standard deviation = 0.05) and "Blue_finger" (standard deviation = 0.04) reflects their morphological overlap with other nail conditions, though performance remains clinically acceptable.

The proposed DAFB model offers significant advantages over existing methods for nail disease classification, especially for high-risk conditions such as acral lentiginous melanoma, achieving perfect recall (1.00) and F1-score (1.00). This performance is critical for clinical applicability, as early diagnosis of melanoma has been shown to improve outcomes for affected patients.[43-45] The DAFB model outperforms static CNNs (using AFB)[10,13], as other models are constrained by fixed hierarchies of feature types, which consequently lead to a plateau in accuracy (~84–89%). Hybrid models (image processing from 7+ deep learning) rely on hand-tuned feature-detection parameters and have not had much success in addressing subtle differences in pathologies (pitting versus clubbing). In contrast, AFB's dual-path attention dynamically recalibrates features, leading to reduced misclassifications in morphologically

Table 4. The hyperparameters for the proposed work

Layer name	Type	Input shape	Output shape	Number of parameters
EfficientNetV2-S Backbone	Pre-trained convolutional neural network	(3, 224, 224)	(1,280, 7, 7)	~7 M (varies)
Stem Conv2D	Conv2D (3 × 3)	(3, 224, 224)	(24, 112, 112)	648
Batch norm	BatchNorm2D	(24, 112, 112)	(24, 112, 112)	48
SiLU activation	SiLU	(24, 112, 112)	(24, 112, 112)	0
MBConv block (×4)	Depthwise separable	(24, 112, 112)	(48, 56, 56)	48 K
MBConv block (×4)	Depthwise separable	(48, 56, 56)	(64, 28, 28)	115 K
MBConv block (×4)	Depthwise separable	(64, 28, 28)	(128, 14, 14)	230 K
MBConv block (×6)	Depthwise separable	(128, 14, 14)	(160, 14, 14)	590 K
MBConv block (×9)	Depthwise separable	(160, 14, 14)	(256, 7, 7)	1.2 M
Adaptive feature blending	Feature enhancement	(1,280, 7, 7)	(1280, 7, 7)	1.6 M
Conv2D 1 × 1	Conv2D (1 × 1)	(1,280, 7, 7)	(640, 7, 7)	819 K
ReLU activation	ReLU	(640, 7, 7)	(640, 7, 7)	0
Conv2D 1 × 1	Conv2D (1 × 1)	(640, 7, 7)	(1,280, 7, 7)	819 K
Sigmoid activation	Sigmoid	(1,280, 7, 7)	(1,280, 7, 7)	0
Element-wise multiplication	Element-wise op	(1,280, 7, 7)	(1,280, 7, 7)	0
Residual addition	Elementwise add	(1,280, 7, 7)	(1,280, 7, 7)	0
Fully connected layers	Classification	(1,280)	(6)	7.7 K
Global average pooling	AdaptiveAvgPool2D	(1,280, 7, 7)	(1,280, 1, 1)	0
Flatten	Flatten	(1,280, 1, 1)	(1,280)	0
Fully connected layer	Linear	(1280)	(6)	7.7 K
Softmax	Softmax	(6)	(6)	0

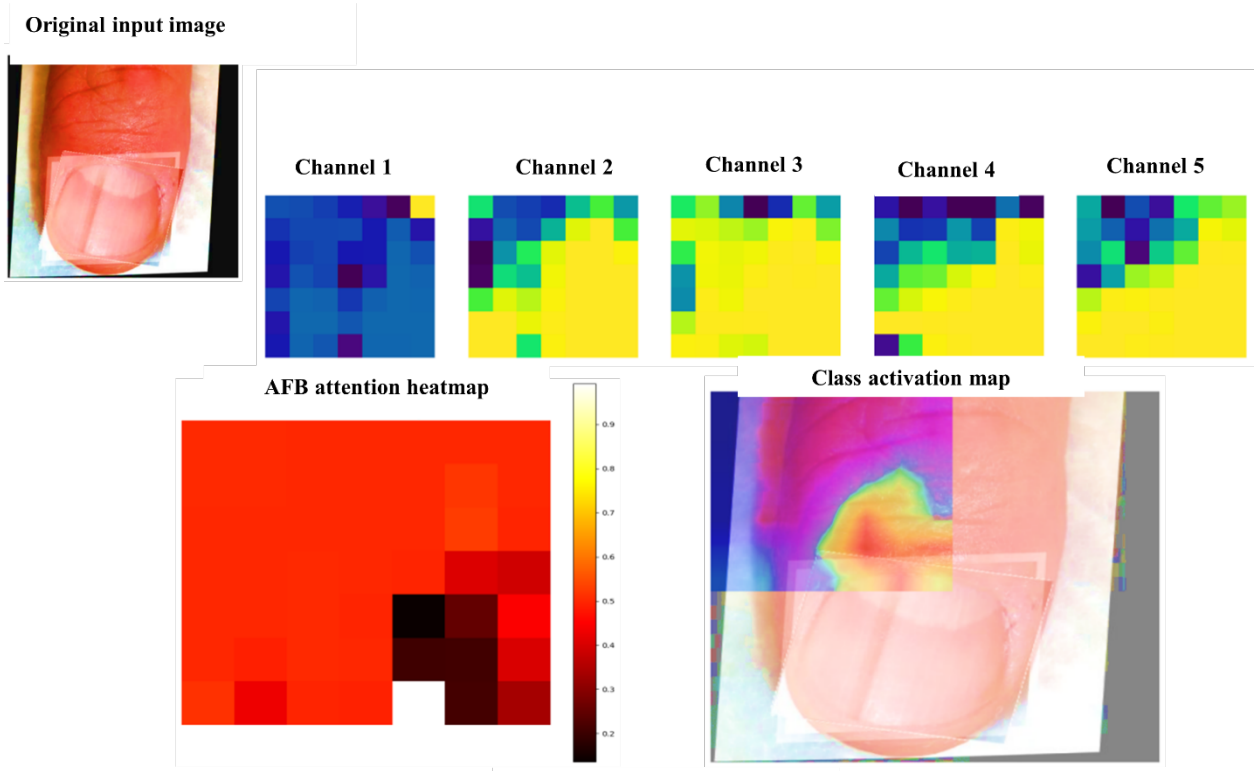

Figure 6. Visualization of feature maps and attention mechanisms in the proposed model. (A) Feature maps before adaptive feature blending (AFB). (B) AFB attention heatmap. (C) Class activation map.

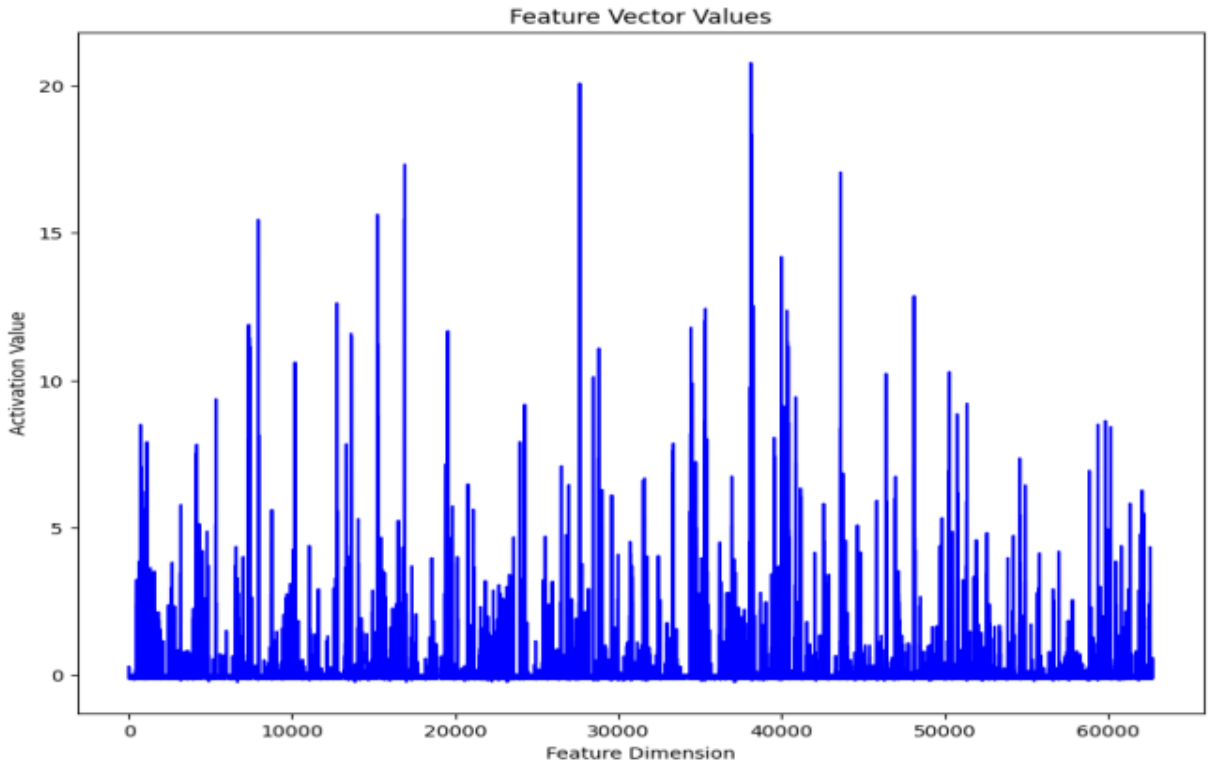

Figure 7. Multi-scale feature analysis and adaptive feature blending (AFB) impact

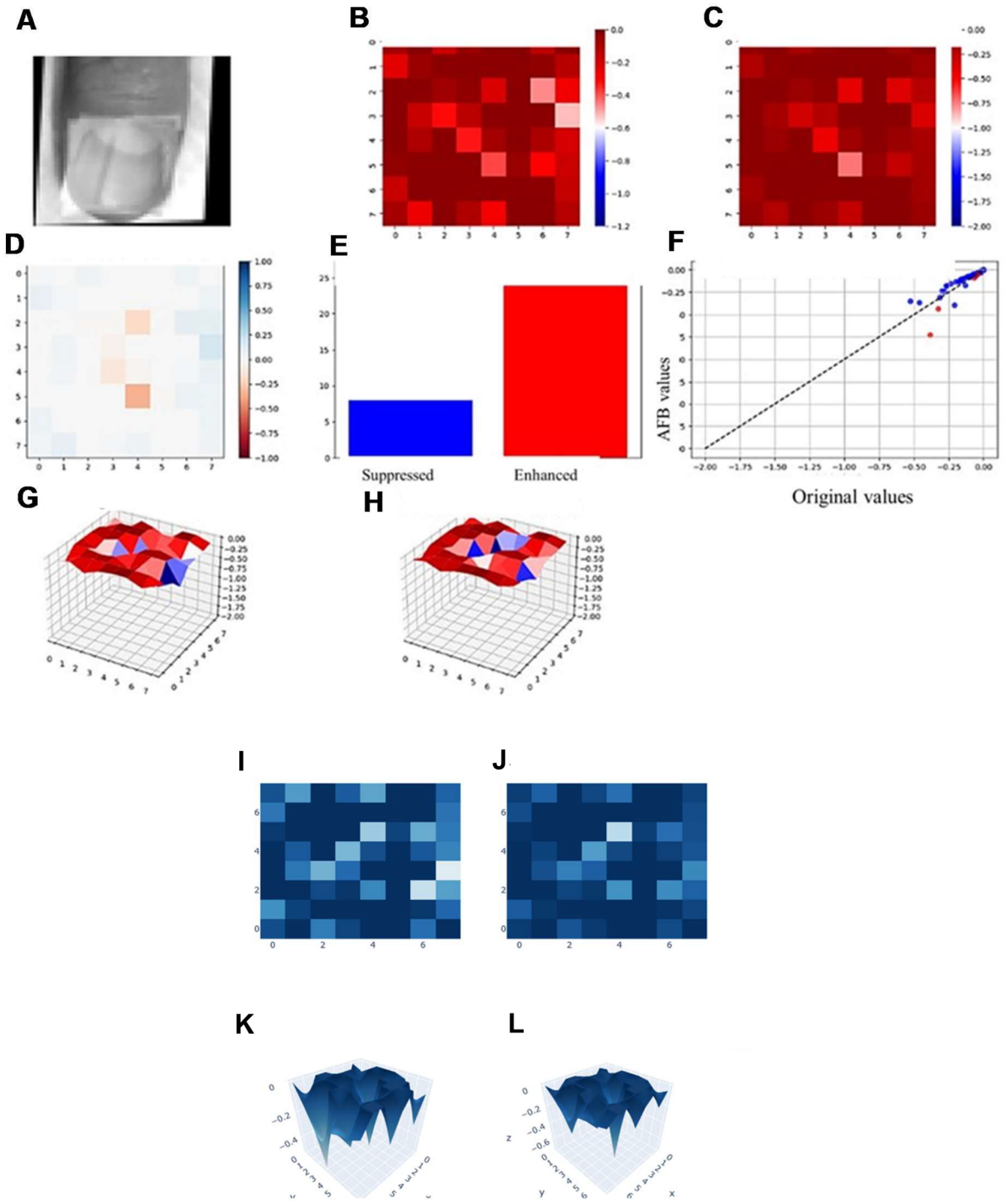

Figure 8. Comparative feature map analysis across attention mechanisms. (A) Clinical nail image. (B) Original features. (C) Adaptive feature blending (AFB)-enhanced features. (D) Feature modifications and (E) statistics. (F) Feature value correlation. (G) Three-dimensional (3D) original features. (H) 3D enhanced features. Interactive visualization of the (I) original features, (J) AFB-enhanced features, and (K & L) attention maps of pathology.

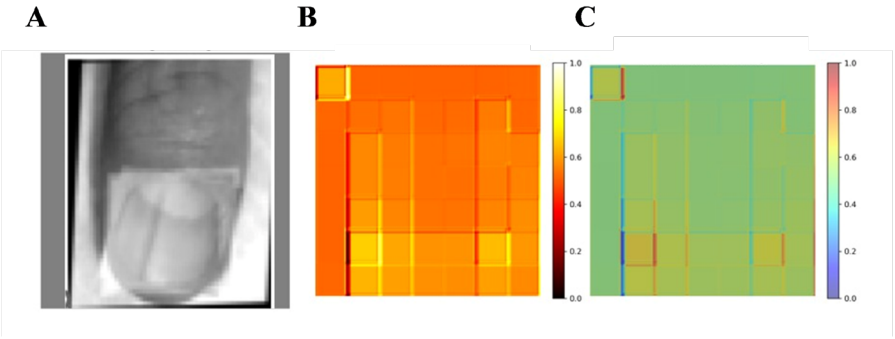

Figure 9. Visualization of spatial attention mechanism: (A) original three-dimensional image, (B) spatial attention map highlighting salient regions, and (C) attention overlay illustrating the contribution of important features on the input image. The results demonstrate that the model focuses on discriminative regions to improve feature representation.

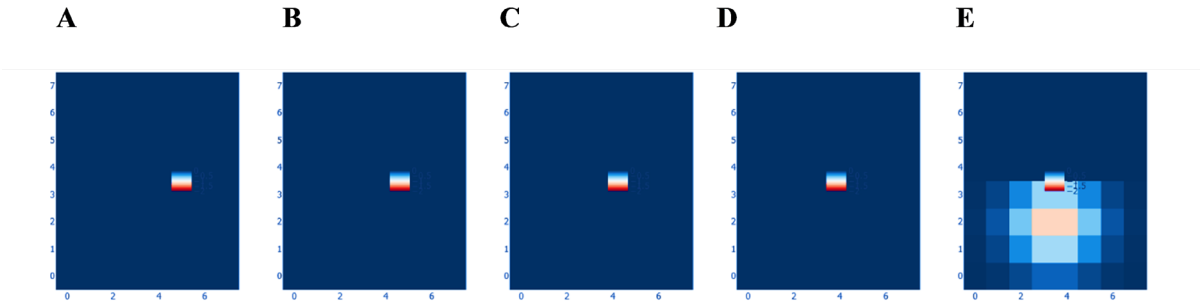

Figure 10. Comparative feature map analysis across attention mechanisms. (A) Adaptive feature blending. (B) Self-attention. (C) Squeeze-and-excitation network. (D) Feature pyramid network. (E) Mixture-of-experts.

Table 5. Summary of the experimental setup

Category	**Details**
Dataset	
Training	6-class nail disease images: acral_lentiginous_melanoma, healthy_nail, onychogryphosis, blue_finger, clubbing, pitting
Validation	Held-out set (same 6 classes)
Augmentations	Random horizontal/vertical flips, color jitter, rotation (±20°), ImageNet normalization
Model architecture	
Backbone	Pretrained EfficientNetV2-S
Custom module	Adaptive feature blending (AFB) before the classification head
Trainable parameters	All layers fine-tuned
Training protocol	
Optimizer	AdamW, learning rate: 0.0001, weight decay: 1×10^{-4}
Loss function	Cross-entropy
Epochs	20
Batch size	32
Hardware	CUDA-enabled GPU (preferred), fallback to CPU

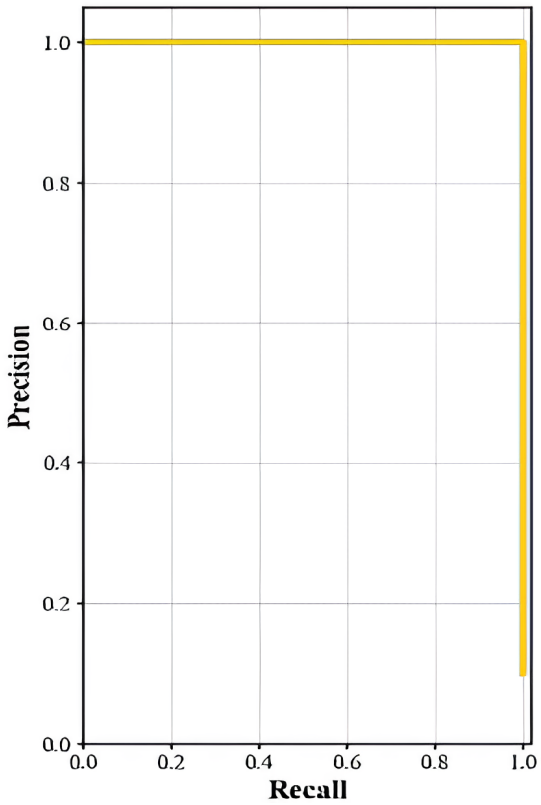

Figure 11. The learning curves for the proposed deep adaptive feature blending framework. Only the "Pitting" and "Blue_finger" classes exhibited slight variations in performance, which makes their curves visible and distinguishable.
Abbreviation: AP: Average precision.

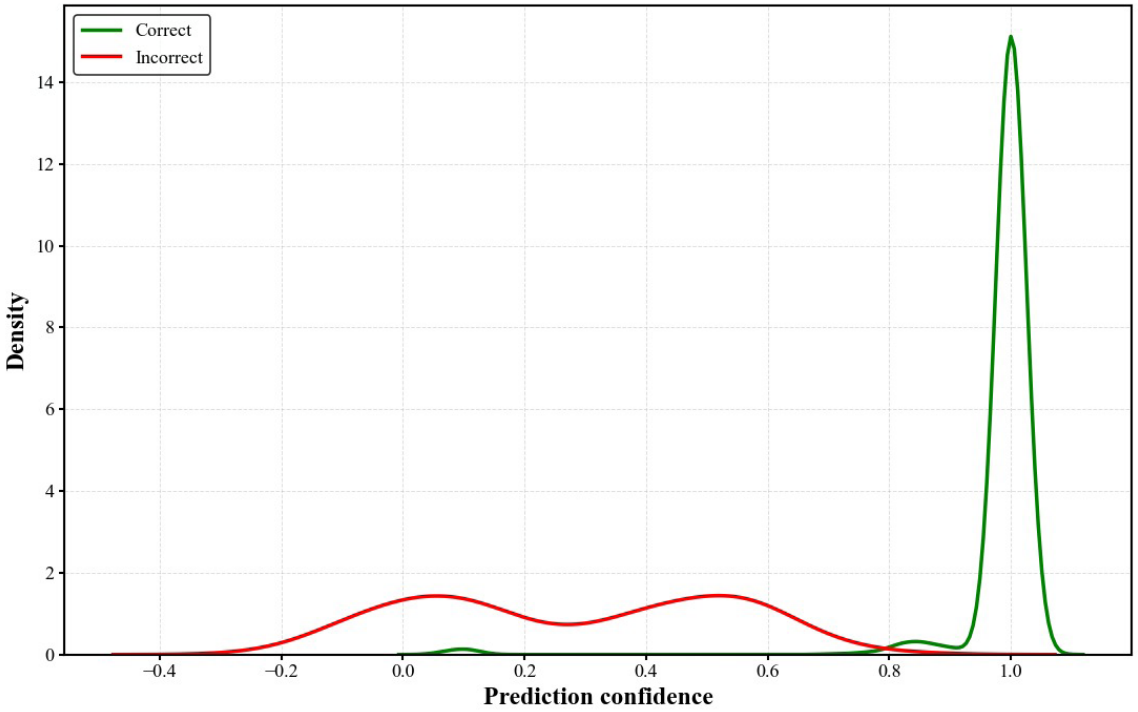

Figure 12. The distribution of model confidence scores for correct vs. incorrect predictions

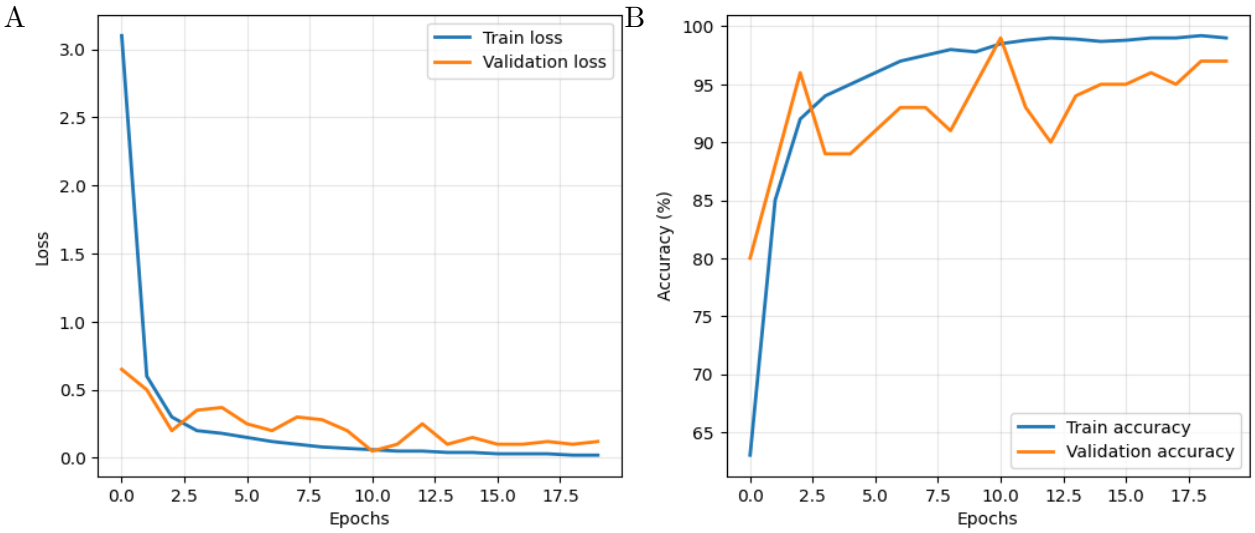

Figure 13. Training and validation performance curves. (A) Loss convergence. (B) Accuracy progression.

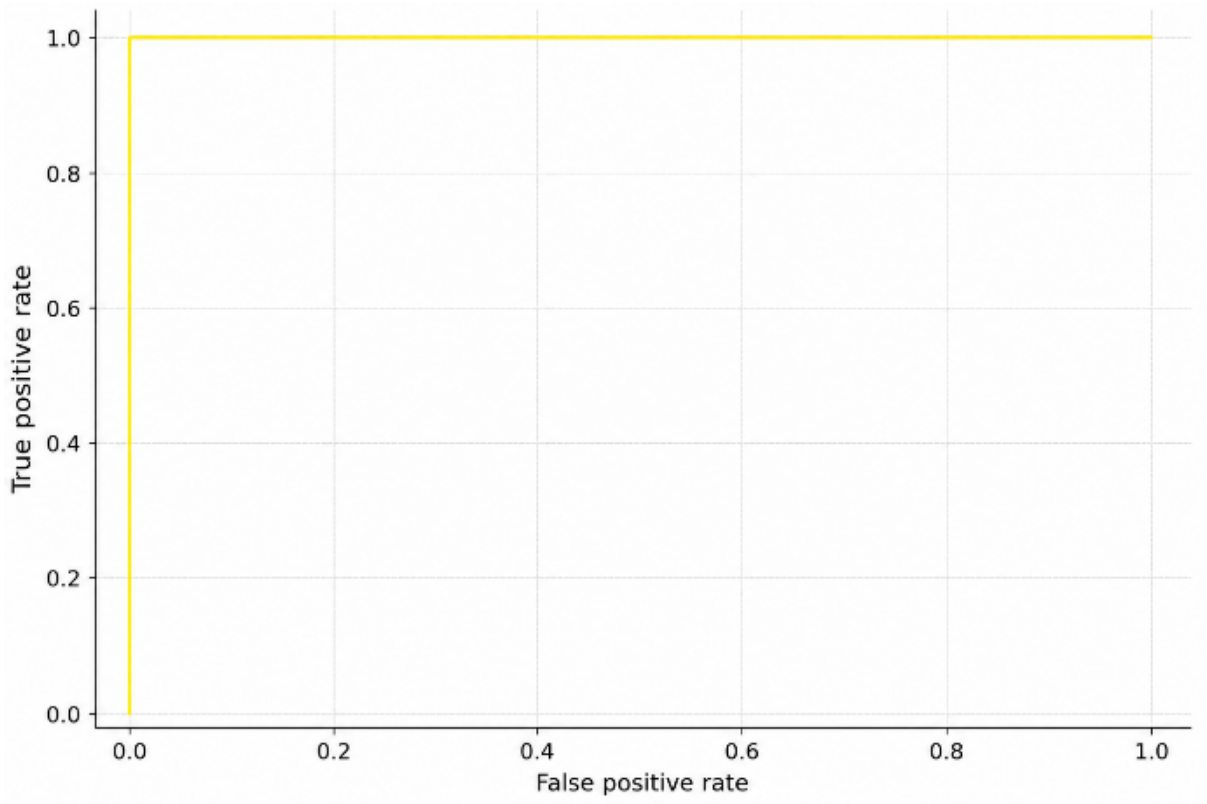

Figure 14. Receiver operating characteristic curve for each nail disease class

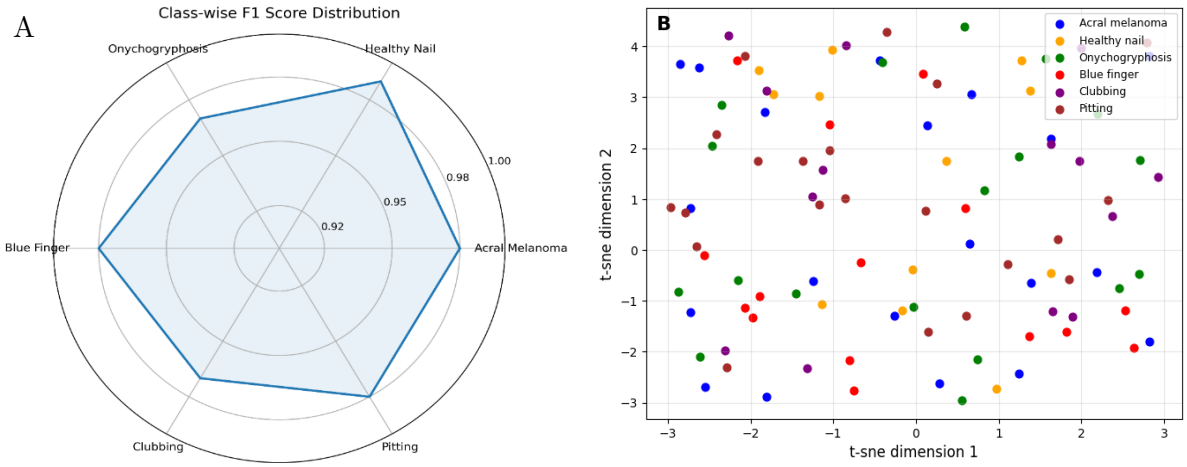

Figure 15. Performance and feature space visualization. (A) F1 scores across diagnostic categories, showing the highest performance for "Healthy_nail" (0.98) and "Acral_lentiginous_melanoma" (0.94). (B) t-distributed stochastic neighbor embedding (SNE) visualization of learned feature embeddings, demonstrating effective separation between pathological clusters.

Table 6. Class-wise F1 scores

Class	**Mean F1 ± standard deviation**	**95% confidence interval**
Onychogyphosis	0.96 ± 0.03	0.93–0.99
Healthy nail	0.98 ± 0.01	0.97–0.99
Blue finger	0.94 ± 0.04	0.90–0.98
Acral lentiginous melanoma	0.99 ± 0.01	0.98–1.00
Pitting	0.95 ± 0.03	0.92–0.98
Clubbing	0.93 ± 0.05	0.88–0.98

Table 7. The proposed classification model performance across nail disease categories

Class	**Precision**	**Recall**	**F1-score**
Acral lentiginous melanoma	1.00	1.00	1.00
Healthy nail	1.00	1.00	1.00
Onychogryphosis	1.00	1.00	1.00
Blue finger	0.90	1.00	0.95
Clubbing	1.00	0.88	0.93
Pitting	0.94	1.00	0.97

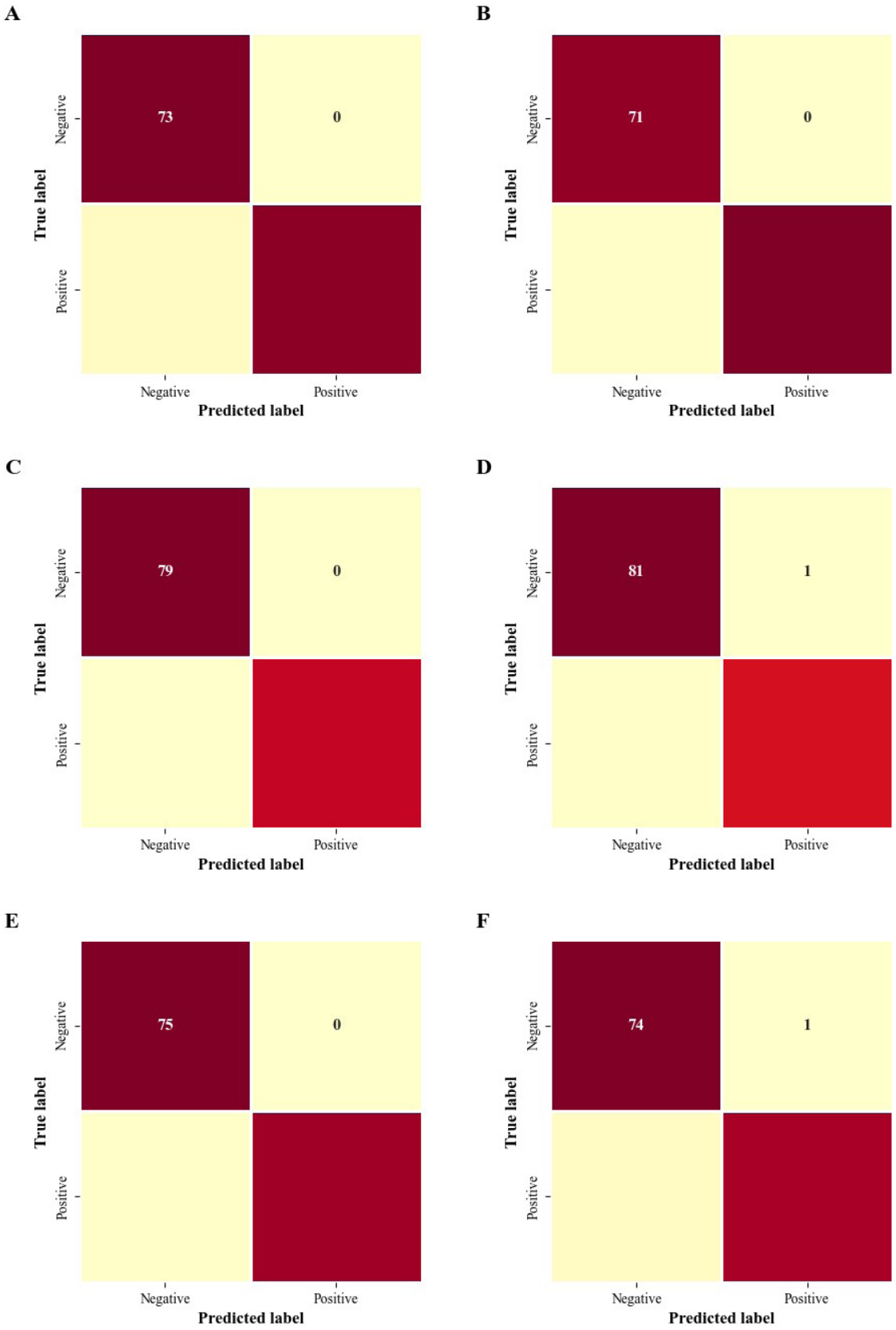

Figure 16. Class-wise confusion matrices for nail disease classification error analysis. (A) Acral melanoma. (B) Healthy nail. (C) Onychogryphosis. (D) Blue finger. (E) Clubbing. (F) Pitting.

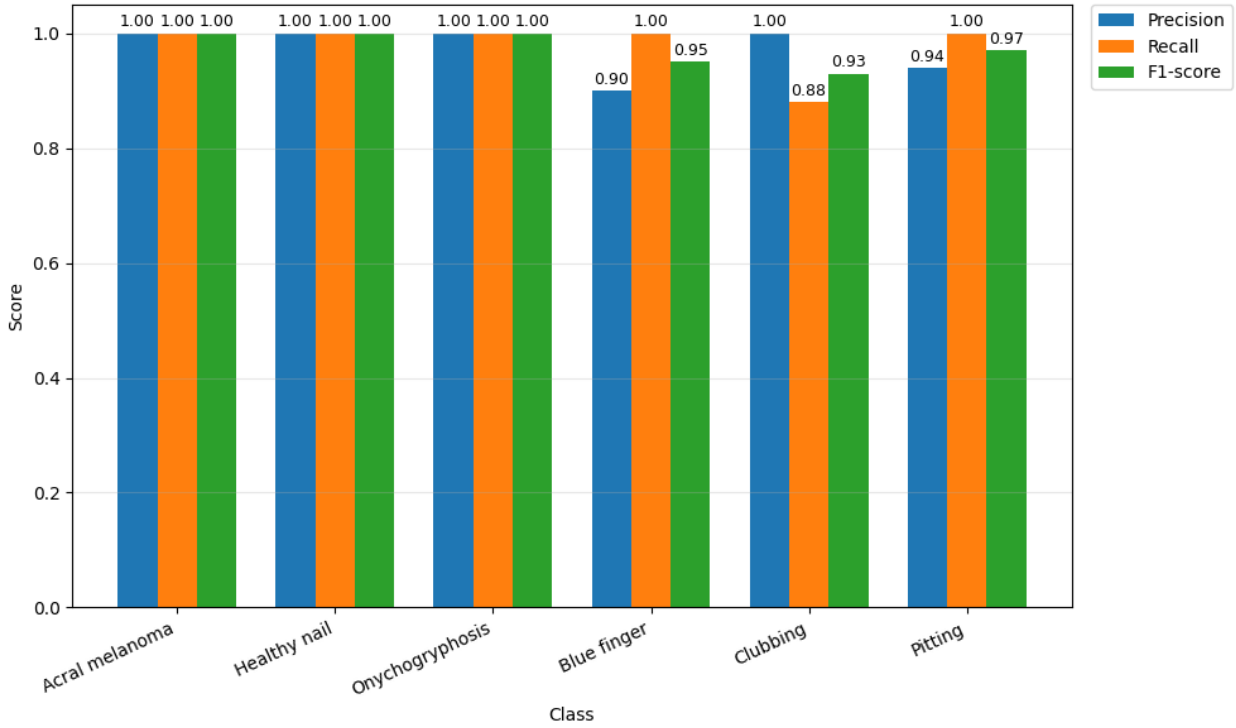

Figure 17. Precision, recall, and F1-score for each class of nail disease

Table 8. Computational efficiency of the modules

Metric	Deep AFB (Proposed)	SE-Net	CBAM
Parameters added	~50 K	~25 K	~75 K
FLOPs per image	0.8 GFLOPs	0.5 GFLOPs	1.2 GFLOPs
Inference time (ms)	12 ms (GPU) / 45 ms (CPU)	8 ms (GPU) / 30 ms (CPU)	18 ms (GPU) / 65 ms (CPU)
Memory usage	1.1 GB	0.7 GB	1.5 GB

Abbreviations: AFB: Adaptive feature blending; CBAM: Convolutional block attention module; CPU: Central processing unit; FLOP: Floating point operation; GPU: Graphics processing unit; SE-Net: Squeeze-and-excitation network.

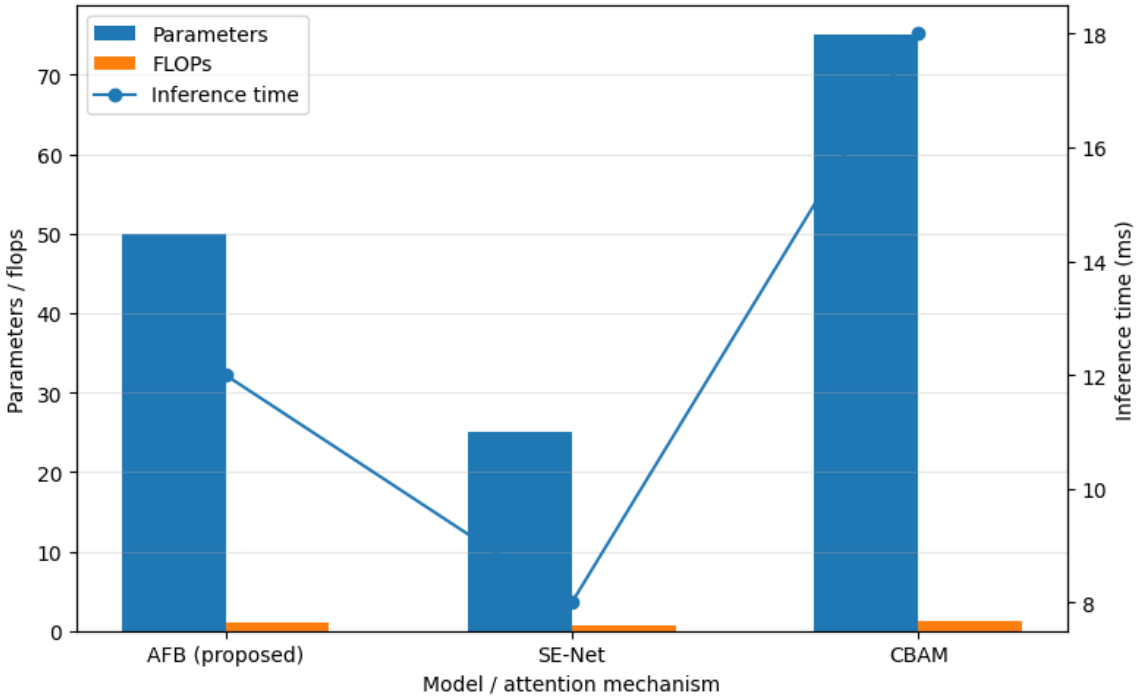

Figure 18. Computational efficiency comparison
Abbreviations: AFB: Adaptive feature blending; CBAM: Convolutional block attention module; FLOP: Floating point operation; SE-Net: Squeeze-and-excitation network.

Table 9. Performance comparison of nail disorder classification models

Model	Attention mechanism	Precision	Recall	F1-score	Accuracy	Param (M)	GFLOPs
Deep AFB (Proposed)	AFB	0.97 ± 0.01	0.98 ± 0.01	0.98 ± 0.01	97.8 ± 0.6%	14.2	2.8
Baseline architectures (No attention)							
ResNet50	N/A	0.88 ± 0.02	0.87 ± 0.02	0.87 ± 0.02	87.6 ± 1.2%	25.6	4.1
DenseNet121	N/A	0.90 ± 0.02	0.89 ± 0.02	0.89 ± 0.02	89.3 ± 1.0%	8.0	2.9
EfficientNetV2-S	N/A	0.92 ± 0.02	0.91 ± 0.02	0.91 ± 0.01	91.7 ± 0.8%	12.5	2.5
ConvNeXt-Tiny	N/A	0.93 ± 0.01	0.92 ± 0.02	0.92 ± 0.01	92.8 ± 0.7%	28.6	4.5
ViT-B/16	N/A	0.92 ± 0.02	0.91 ± 0.02	0.91 ± 0.02	92.1 ± 1.1%	86.6	17.6
Attention mechanisms (on EfficientNetV2-S)							
EfficientNetV2-S + SE-Net [A]	SE-Net	0.94 ± 0.01	0.93 ± 0.01	0.93 ± 0.01	93.5 ± 0.7%	13.1	2.7
EfficientNetV2-S + CBAM [B]	CBAM	0.94 ± 0.01	0.94 ± 0.01	0.94 ± 0.01	94.2 ± 0.6%	13.4	2.8
EfficientNetV2-S + AFB (Ours)	AFB	0.97 ± 0.01	0.98 ± 0.01	0.98 ± 0.01	97.8 ± 0.6%	14.2	2.8

Abbreviations: AFB: Adaptive feature blending; CBAM: Convolutional block attention module; GFLOP: Giga floating point operation; SE-Net: Squeeze-and-excitation network.

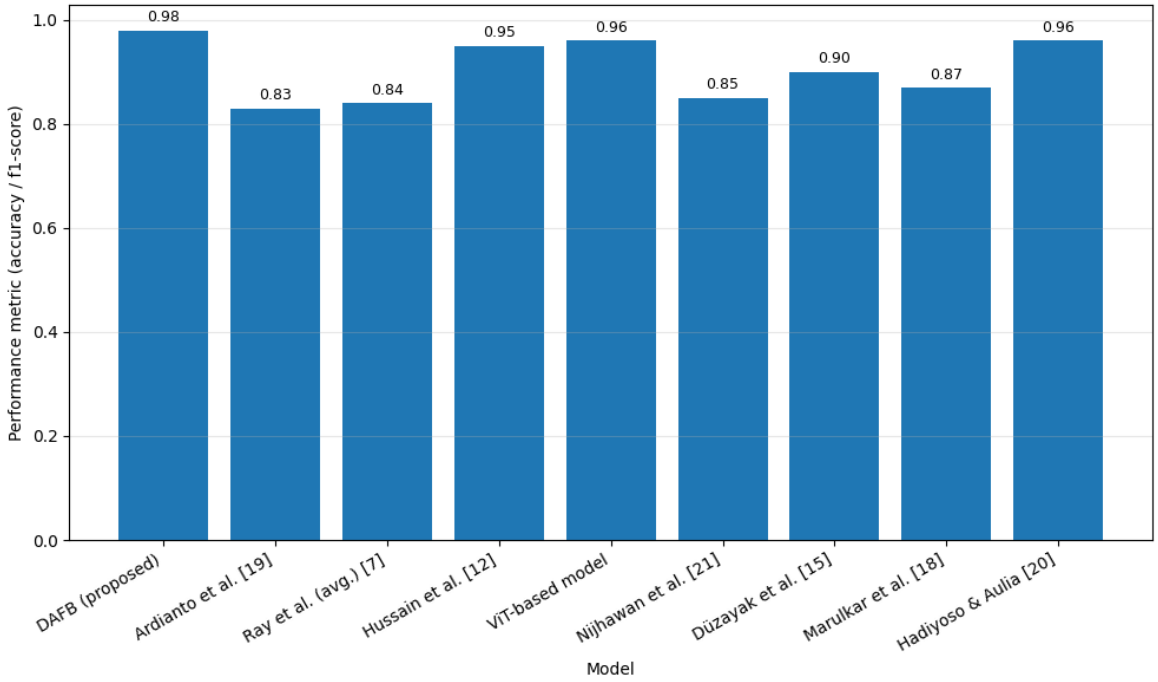

Figure 19. Comparison of nail disorder classification models
Abbreviation: DAFB: Deep adaptive feature blending.

similar conditions (Blue_finger precision: 0.90 vs. 0.72 in[7]). Although the model performs well in common pathologies (melanoma, pitting), its performance in ultra-rare pathologies (subungual exostosis, $n < 5$) remains unvalidated because of insufficient samples.

5. Conclusion

Nail diseases present significant diagnostic challenges due to their morphological variability, subtle visual differences, and overlapping clinical patterns, which may lead to misdiagnosis or delayed treatment. Traditional diagnostic approaches rely heavily on subjective interpretation by dermatologists, which can vary depending on expertise. To address these challenges, this study introduced the DAFB framework, which integrates EfficientNetV2-S with an AFB module to enhance feature representation and classification performance. The experimental results demonstrate that the proposed DAFB model achieved strong performance, with a validation accuracy of 97.8%, and demonstrated improved capability to capture subtle pathological patterns compared to baseline and attention-based methods. Additionally, feature visualization techniques provide insights into the model's decision-making process, supporting its interpretability. Despite these promising results, it is important to note that the current evaluation is limited to a single dataset with a relatively small validation set and no external testing. Therefore, the findings should be considered preliminary and not yet indicative of clinical deployment readiness. Future work should focus on validating the proposed framework using larger, multi-center datasets with diverse patient populations, and on incorporating external evaluation protocols and clinically verified annotations. In summary, the proposed DAFB framework represents a promising step toward automated nail disease classification, but further validation is required before considering real-world clinical application.

Acknowledgments

None.

Funding

None.

Conflict of interest

The authors declare no conflict of interest.

Author contributions

Conceptualization: Nora Elrashidy, Zahraa Tarek, Jawhara Aljabri
Formal analysis Eman Allogmani, Jawhara Aljabri
Methodology: Esraa Hassan
Writing – original draft: Esraa Hassan, Nora Elrashidy, Zahraa Tarek
Writing – review & editing: Samar Elbedwehy, Rana Albelaihi

Availability of data

Data will be made available upon request to the corresponding author.

AI tools statement

Not applicable.

References

1. Alharbi LA. Artificial Rabbits Optimizer With Machine Learning Based Emergency Department Monitoring and Medical Data Classification at KSA Hospitals. *IEEE Access.* 2023;11:59133-59141.

   https://www.doi.org/10.1109/access.2023.3284390

2. Alanazi AS, Mezher MA. Using Machine Learning Algorithms for Prediction of Diabetes Mellitus. In: Proceedings of the 2020 International Conference on Computing and Information Technology (ICCIT-1441). IEEE; 2020:1-3.

   https://www.doi.org/10.1109/iccit-144147971.2020.9213708

3. Manimurugan S, Al-Mutairi S, Aborokbah MM, Chilamkurti N, Ganesan S, Patan R. Effective Attack Detection in Internet of Medical Things Smart Environment Using a Deep Belief Neural Network. *IEEE Access.* 2020;8:77396-77404.

   https://www.doi.org/10.1109/access.2020.2986013

4. Taouali O, Bacha S, Ben Abdellafou K, *et al.* Intelligent Intrusion Detection System for the Internet of Medical Things Based on Data-Driven Techniques. *Comput Syst Sci Eng.* 2023;47(2):1593-1609.

   https://www.doi.org/10.32604/csse.2023.039984

5. Sechi A, Wortsman X, Tosti A, Iorizzo M. Advances in image-based diagnosis of nail disorders. *Acad Dermatol Venereol.* 2024;39(4):759-774.

   https://www.doi.org/10.1111/jdv.20309

6. Almutairi SM, Manimurugan S, Aborokbah MM, Narmatha C, Ganesan S, Karthikeyan P. An Efficient USE-Net Deep Learning Model for Cancer Detection. *Int J Intell Syst.* 2023;2023(1), 8509433.

   https://www.doi.org/10.1155/2023/8509433

7. Hamim MA, Sajim SH, Ur Rahman F, Tanmoy FM. Multiple Skin-Disease Classification Based on Machine Vision Using Transfer Learning Approach. In: Proceedings of the 2023 14th International Conference on Computing Communication and Networking Technologies (ICCCNT). IEEE; 2023:1-8.

   https://www.doi.org/10.1109/icccnt56998.2023.10307018

8. Gaurav V, Grover C, Tyagi M, Saurabh S. Artificial Intelligence in Diagnosis and Management of Nail Disorders: A Narrative Review. *Indian Dermatol Online J.* 2024;16(1):40-49.

   https://www.doi.org/10.4103/idoj.idoj_460_24

9. Wang Z, Jiang JX, Wang HR, Zhou L, Li Y. Localized Adaptive Style Mixing for feature statistics manipulation in medical image translation with limited Data. *Expert Syst Appl.* 2025;277:127217.

   https://www.doi.org/10.1016/j.eswa.2025.127217

10. Xu Y, Zhang T. Boundless Across Domains: A New Paradigm of Adaptive Feature and Cross-Attention for Domain Generalization in Medical Image Segmentation. *arXiv.*

    https://www.doi.org/10.48550/ARXIV.2411.14883

11. Zhao H, Zhang X, Gao Y, *et al.* Diagnostic performance of EfficientNetV2-S method for staging liver fibrosis based on multiparametric MRI. *Heliyon.* 2024;10(15):e35115.

    https://www.doi.org/10.1016/j.heliyon.2024.e35115

12. Al Moteri M, Mahesh TR, Thakur A, Vinoth Kumar V, Khan SB, Alojail M. Enhancing accessibility for improved diagnosis with modified EfficientNetV2-S and cyclic learning rate strategy in women with disabilities and breast cancer. *Front Med.* 2024;11.

    https://www.doi.org/10.3389/fmed.2024.1373244

13. Zhao J, Feng X, Tran MK, Fowler M, Ouyang M, Burke AF. Battery safety: Fault diagnosis from laboratory to real world. *J Power Sources.* 2024;598:234111.

    https://www.doi.org/10.1016/j.jpowsour.2024.234111

14. Hassan E, Saber A, Elbedwehy S. Knowledge distillation model for Acute Lymphoblastic Leukemia Detection: Exploring the impact of nesterov-accelerated adaptive moment estimation optimizer. *Biomed Signal Process Control.* 2024;94:106246.

https://www.doi.org/10.1016/j.bspc.2024.106246

15. Elbedwehy S, Hassan E, Saber A, Elmonier R. Integrating neural networks with advanced optimization techniques for accurate kidney disease diagnosis. *Sci Rep*. 2024;14(1).

https://www.doi.org/10.1038/s41598-024-71410-6

16. Shandilya G, Gupta S, Bharany S, *et al.* Autonomous detection of nail disorders using a hybrid capsule CNN: a novel deep learning approach for early diagnosis. *BMC Med Inform Decis Mak*. 2024;24(1).

https://www.doi.org/10.1186/s12911-024-02840-5

17. Hadiyoso S, Aulia S. Classification of Koilonychia, Beaus Lines, and Leukonychia based on Nail Image using Transfer Learning VGG-16. *JRE*. 2022;18(2).

https://www.doi.org/10.17529/jre.v18i2.25694

18. Saber A, Elbedwehy S, Awad WA, Hassan E. An optimized ensemble model based on meta-heuristic algorithms for effective detection and classification of breast tumors. *Neural Comput Appl*. 2024;37(6):4881-4894.

https://www.doi.org/10.1007/s00521-024-10719-9

19. Ardianto R, Yusuf D, Sumantri RBB, Febrina D, Al-Hakim RR, Ariyanto ASS. Bioinformatics-driven deep learning for nail disease diagnosis: A novel approach to improve healthcare outcomes. *BIO Web Conf*. 2025;152:01024.

https://www.doi.org/10.1051/bioconf/202515201024

20. Hussain M, Fiza M, Khalil A, *et al.* Transfer learning-based quantized deep learning models for nail melanoma classification. *Neural Comput Appl*. 2023;35(30):22163-22178.

https://www.doi.org/10.1007/s00521-023-08925-y

21. Krizhevsky A, Sutskever I, Hinton GE. ImageNet Classification with Deep Convolutional Neural Networks. In: Proceedings of the NIPS'12: Proceedings of the 26th International Conference on Neural Information Processing Systems - Volume 1. 2012;60(6):84-90.

22. Ren Q, Wang Y, Xu J, Hou F, Cui G, Ding G. REN-GAN: Generative adversarial network-driven rebar clutter elimination network in GPR image for tunnel defect identification. *Expert Systems with Applications*. 2024;255:124395.

https://www.doi.org/10.1016/j.eswa.2024.124395

23. Zarpalas D, Gkontra P, Daras P, Maglaveras N. Segmentation through a local and adaptive weighting scheme, for contour-based blending of image and prior information. In: Proceedings of the 2012 25th IEEE International Symposium on Computer-Based Medical Systems (CBMS). IEEE; 2012:1-4.

https://www.doi.org/10.1109/cbms.2012.6266319

24. Abd El-Aziz AA, Mahmood MA, Abd El-Ghany S. A Robust EfficientNetV2-S Classifier for Predicting Acute Lymphoblastic Leukemia Based on Cross Validation. *Symmetry*. 2024;17(1):24.

https://www.doi.org/10.3390/sym17010024

25. Cheng R, Razani R, Taghavi E, Li E, Liu B. $(AF)^2$-S3Net: Attentive Feature Fusion with Adaptive Feature Selection for Sparse Semantic Segmentation Network. In: Proceedings of the 2021 IEEE/CVF Conference on Computer Vision and Pattern Recognition (CVPR). IEEE; 2021:12542-12551.

https://www.doi.org/10.1109/cvpr46437.2021.01236

26. Liu T, Luo R, Xu L, *et al.* Spatial Channel Attention for Deep Convolutional Neural Networks. *Mathematics*. 2022;10(10):1750.

https://www.doi.org/10.3390/math10101750

27. Alnaggar MH, El-Dosuky MA, Rashad MZ. A Novel Multimodal Biometric Template Security Based on Nano-Scale Reaction-Diffusion Morphogenesis. *J Comput Theor Nanosci*. 2018;15(6):1979-1982.

https://www.doi.org/10.1166/jctn.2018.7522

28. Hinton G, Vinyals O, Dean J. Distilling the knowledge in a neural network. *arXiv*. 2015. https://arxiv.org/abs/1503.02531

29. Yousef Saleh Al Alawi, Albalawi IAJ, Alamrani SAS, *et al.* Knowledge of diabetic foot care management among medical students at Tabuk University, Tabuk, Saudi Arabia. *SMHJ*. 2023;3(2):58-71.

https://www.doi.org/10.54293/smhj.v3i2.73

30. Alqahtani M, Alanazi A, Elbadawi A, Qahtani A, Alqahtani M, Alanazi A. Prevalent and risk factors of depression among Saudi medical residents in the Tabuk City, Saudi Arabia. *IJMDC*. Published online 2024:2347-2351.

https://www.doi.org/10.24911/ijmdc.51-1726583030

31. Alatawi MN. Machine Learning-Based Usage Evaluation Strategy for Mobile E-Learning Systems in KSA Institutions. In: Proceedings of the 2023 3rd International Conference on Computing and Information Technology (ICCIT). IEEE; 2023:510-516.

https://www.doi.org/10.1109/iccit58132.2023.10273888

32. Almasoudi FM. Grid Distribution Fault Occurrence and Remedial Measures Prediction/Forecasting through Different Deep Learning Neural Networks by Using Real Time Data from Tabuk City Power Grid. *Energies*. 2023;16(3):1026.

https://www.doi.org/10.3390/en16031026

33. Ibrahim M, Ali M, Ahmed M, *et al.* A Low-Cost Approach for Drowning Detection and Alertness. *Egypt J Artif Intell.* 2024;3(1):0-0.

https://www.doi.org/10.21608/ejai.2024.223796.1012

34. Hassan E, Bhatnagar R, Shams MY. Advancing Scientific Research in Computer Science by ChatGPT and LLaMA—A Review. In: *Smart Innovation, Systems and Technologies*. Singapore: Springer Nature; 2023:23-37.

https://www.doi.org/10.1007/978-981-99-6774-2_3

35. Hassan E, El-Rashidy N, Elbedwehy S, Abd El-Hafeez T, Saber A, Shams MY. Exploring the frontiers of image super-resolution: a review of modern techniques and emerging applications. *Neural Comput Appl.* 2025;37(22):17913-17961.

https://www.doi.org/10.1007/s00521-025-11331-1

36. Hassan E, Bhatnagar R, El-Hafeez TA, Shams MY. Detection of Suicide and Depression for Early Intervention and Initiative-taking Mental Healthcare. In: Proceedings of the 2025 7th International Conference on Signal Processing, Computing and Control (ISPCC). IEEE; 2025:99-104.

https://www.doi.org/10.1109/ispcc66872.2025.11039547

37. Shams MY, Hassan E, Gamil S, *et al.* Skin Disease Classification: A Comparison of ResNet50, MobileNet, and Efficient-B0. *J Curr Multidiscip Res.* 2025;1(1):1-7.

https://www.doi.org/10.21608/jcmr.2025.327880.1002

38. Saber A, Hassan E, Elbedwehy S, Awad WA, Emara TZ. Leveraging ensemble convolutional neural networks and metaheuristic strategies for advanced kidney disease screening and classification. *Sci Rep.* 2025;15(1).

https://www.doi.org/10.1038/s41598-025-93950-1

39. Marode TP, Bhangdiya VK, Nemane S, *et al.* Artificial Intelligence Meets Nail Diagnostics: Emerging Image-Based Sensing Platforms for Non-Invasive Disease Detection. *Bioengineering.* 2026;13(1):75.

https://www.doi.org/10.3390/bioengineering13010075

40. Zhou P, Xie X, Lin Z, Yan S. Towards Understanding Convergence and Generalization of AdamW. *IEEE Trans Pattern Anal Mach Intell.* 2024;46(9):6486-6493.

https://www.doi.org/10.1109/tpami.2024.3382294

41. Eisa MM, Alnaggar MH. Hybrid Rough-Genetic Classification Model for IoT Heart Disease Monitoring System. In: *Lecture Notes in Networks and Systems*. Singapore: Springer; 2021:437-451.

https://www.doi.org/10.1007/978-981-16-2275-5_27

42. Abdella M, Hawash A, Zahran O, *et al.* Smart Tour Guide: A Novel Artificial Intelligence System for Replacing Human Guides in Cultural Heritage Sites. *Egypt J Artif Intell.* 2024;3(1):0-0.

https://www.doi.org/10.21608/ejai.2024.226751.1017

43. Abbas S, Alsubai S, Haque MIU, *et al.* Active Machine Learning for Heterogeneity Activity Recognition Through Smartwatch Sensors. *IEEE Access.* 2024;12:22595-22607.

https://www.doi.org/10.1109/access.2024.3362676

44. Almurtadha Y, Mohammed OS, Mirghani H, Ghaleb M. Investigating the Relationship Between Medicine Student's Lifestyle and Their Academic Performance. In: *Lecture Notes in Networks and Systems*. Springer International Publishing; 2021:455-464.

https://www.doi.org/10.1007/978-3-030-85990-9_37

45. Hassan Abbas Gondal C, Irfan M, Shafique S, Salman Bashir M, Ahmed M, M.Alshehri O, *et al.* Automated Leukemia Screening and Sub-types Classification Using Deep Learning. *Comput Syst Sci Eng.* 2023;46(3):3541-3558.

https://www.doi.org/10.32604/csse.2023.036476

Nora El Rashidy is a researcher and academic specializing in artificial intelligence, machine learning, medical image analysis, and intelligent healthcare systems. Her research interests include deep learning, explainable AI, digital health technologies, and predictive analytics for biomedical applications.
https://orcid.org/0000-0001-8177-9439

Eman Allogmani is a researcher in computer science with interests in artificial intelligence, data analytics, and smart healthcare technologies. Her work focuses on intelligent computational frameworks, machine learning models, and AI-driven decision-support systems.
https://orcid.org/0009-0004-0326-8405

Samar Elbedwehy is an academic researcher whose expertise includes artificial intelligence, deep learning, bioinformatics, and medical data analysis. Her research contributions involve intelligent healthcare systems, computational intelligence, and advanced AI methodologies for biomedical applications.
https://orcid.org/0000-0002-2187-0174

Jawhara Aljabri is a researcher interested in intel-

ligent systems, data science, and emerging artificial intelligence technologies. Her research focuses on machine learning applications, healthcare informatics, and smart computational solutions.
https://orcid.org/0000-0001-6476-4374

Rana Albelaihi is a researcher in artificial intelligence and computer science with interests in deep learning, data-driven healthcare systems, and intelligent medical technologies. Her work includes AI-based prediction systems and advanced computational analysis.
https://orcid.org/0000-0002-5208-9743

Zahraa Tarek is a researcher specializing in artificial intelligence, machine learning, and intelligent biomedical applications. Her research interests include medical imaging, computational intelligence, and AI-enabled healthcare analytics.
https://orcid.org/0000-0001-9389-2850

Esraa Hassan is a researcher in artificial intelligence and computational sciences with expertise in deep learning, medical image analysis, continual learning, and intelligent healthcare systems. Her research focuses on AI-driven diagnostic frameworks, multimodal learning, explainable AI, and adaptive intelligent systems for biomedical and clinical applications.
https://orcid.org/0000-0002-1021-717X

An International Journal of Optimization and Control: Theories & Applications (https://accscience.com/journal/ijocta)